RESEARCH ARTICLE

Feasibility of integrated high-wavenumber Raman imaging and fingerprint Raman spectroscopy for fast margin assessment in breast cancer surgery

Zhiyu Liao[1] | **Maria Giovanna Lizio**[1] | **Christopher Corden**[1] | **Hazem Khout**[2] | **Emad Rakha**[3] | **Ioan Notingher**[1]

[1]School of Physics and Astronomy, University of Nottingham, Nottingham, UK

[2]Nottingham Breast Institute, Nottingham University Hospitals NHS Trust, Nottingham, UK

[3]Division of Oncology, School of Medicine, University of Nottingham, Nottingham, UK

Correspondence
Ioan Notingher, School of Physics and Astronomy, University of Nottingham, Nottingham NG7 2RD, UK.
Email: ioan.notingher@nottingham.ac.uk

Abstract

Intraoperative assessment of surgical margins remains one of the main challenges in cancer surgery. Raman spectroscopy can detect cancer cells with high accuracy, but it is time-consuming. In this paper, we investigated a selective-sampling Raman spectroscopy approach, based on high wavenumber (HW) Raman imaging (spectral range 2,500–3,500 cm^{-1}) and fingerprint Raman spectroscopy (spectral range 600–1,800 cm^{-1}), to reduce the overall tissue analysis time while maintaining high diagnostic accuracy. HW Raman mapping was used as a first step to identify the adipose tissue regions based on the C–H stretching bands at 2,700–2,950 cm^{-1}. As residual tumors are typically found in nonadipose tissue, an algorithm was developed to allocate sampling points for fingerprint Raman spectroscopy at locations corresponding to low intensity in the HW-Raman maps. Preliminary results show that HW-Raman imaging based on a 671 nm laser is effective and fast for mapping of adipose tissue in breast resections, with typical imaging times of 2 min for tissue areas as large as 2×2 cm^2 areas. Albeit the remaining high fluorescence background in the fingerprint region prevents the use of single 671-nm laser, the HW Raman imaging can be still exploited in combination with 785-nm excitation Raman spectroscopy for identifying residual tumor. Although this study demonstrates the feasibility of this approach, further improvements, such as using single element detectors for HW Raman imaging, are required to increase the analysis speed further towards intraoperative use in the routine clinical setting.

KEYWORDS

breast cancer, intraoperative Raman spectroscopy, selective sampling Raman spectroscopy

1 | INTRODUCTION

Breast conserving surgery (BCS) is widely used for treating patients with breast cancers.[1] The main aim of surgery is to remove the tumor while conserving surrounding healthy tissue. The completeness of tumor resection is usually confirmed postoperatively by histopathological examination of fixed tissue. Intraoperative assessment of margins can save up to 40% of BCS patients a second surgical intervention by providing information real-time information to surgeons on whether the entire tumor has been excised or not. Although frozen sections examination can be helpful, it is very challenging to examine the whole surface area of the excised margin and is becoming less common due to availability of pathologists. Current intraoperative imaging of the surgical specimen can help surgeons to excise further tissue. However, the available imaging modalities rely on simple X-rays which lack accuracy. Reports indicate that in about 20% of cases histology detects positive margins, and additional surgeries are required to achieve complete excision.[2,3] There is a need for an accurate and fast tool for intraoperative assessment of surgical margin to aid surgeons in achieving complete resection.

Raman spectroscopy is a highly sensitive optical technique that can be used to measure the molecular composition of tissue without requiring labelling or other contrast enhancing agents.[4] The developments in Raman spectroscopy for intraoperative assessment of surgical margins in cancer surgery have been recently reviewed.[5] Different modalities of Raman spectroscopy, operating in the fingerprint region (600–1,800 cm^{-1}), have been reported in the literature for the assessment of breast specimens, reporting sensitivity and specificity typically higher than 90%,[6] including handheld fiber probes for in vivo point measurements[7,8] and spatially offset Raman spectroscopy (SORS) for detection of positive margins in unsectioned breast resections.[9,10] However, these handheld probes are operator-dependent and can miss small residual tumors (e.g., ductal carcinoma in situ). Raster-scanning imaging based on spontaneous Raman microscopy has the spatial accuracy and molecular specificity needed but requires long acquisition times, making this technique impractical for intraoperative use. One approach for reducing the acquisition time is surface-enhanced Raman spectroscopy (SERS), where the speed of imaging significantly boosted by the signal enhancement. Kang et al[11] demonstrated detection of tumor on the excision surface with 89% sensitivity and 92% specificity by using gold nanoparticles functionalized with reporter SERS labels and monoclonal antibodies targeting specific biomarkers.

An alternative approach to reduce analysis time is selective-sampling Raman spectroscopy, which uses spatial information of the sample to guide Raman spectroscopy to the regions more likely to contain tumor, thus reducing the overall number of Raman measurements.[12–16] This approach has the advantage that no exogenous labels are required, making it potentially simpler for clinical use. In a previous study, we developed a selective-sampling technique that combined high-resolution wide-field auto-fluorescence (AF) microscopy and fingerprint Raman spectroscopy (700–1,800 cm^{-1} Raman shift region) to detect ductal carcinomas in frozen breast microsections (5 × 5 mm^2).[14] More recently, confocal AF-Raman spectroscopy combined with more efficient data processing algorithms enabled the analysis of larger tissues areas (4 × 6.5 cm^2 area) with acquisition times of 12–24 min, achieving 95% sensitivity and 82% specificity in an independent test on 121 samples from 107 patients (including 51 fresh, whole excision specimens).[17] Although the confocal AF was effective in segmenting the tissue images based on AF intensity, it was not able to reliably identify the regions of adipose tissue. As most of the surface area of breast excision specimens is composed of adipose tissue, a large number of Raman fingerprint spectra were from adipose tissue areas, increasing analysis time, even though these rarely contain tumor.

In this study, we propose an improved method for analyzing the margins of breast resection specimens by using the high-wavenumber (HW) (2,700–3,500 cm^{-1}) and fingerprint Raman spectral regions. The confocal AF imaging was replaced by HW Raman mapping to detect adipose tissue based on the lipid bands at the 2,800–3,100 cm^{-1}. HW Raman spectroscopy has been proposed for fast tumor diagnosis in head-and-neck cancer.[18–20] Here, HW is used only for screening out adipose tissue, and the final diagnosis is then performed using fingerprint Raman spectroscopy measurements at the remaining non-adipose tissue areas. This approach has the advantage of targeting the fingerprint Raman measurements more effectively to the nonadipose tissue areas, which are associated with stroma, benign, or malignant tumor.

2 | METHODS

2.1 | Tissue samples

Breast tissue blocks with sizes in the ranges 4 × 6 mm^2 to 20 × 20 mm^2 (thickness of ∼2 mm) were cut from breast resection during mastectomy and stored at −20°C. Although surgical practice involved injection of blue dye

in subareolar region in order to aid the identification of sentinel lymph nodes, no dye was detected at the margin of the wide local excision. Prior to Raman spectroscopy experiments, samples were thawed at room temperature. Ethical approval was granted through the Nottingham Health Science Biobank (NHSB, REC reference 15/NW/0685), and informed consent was obtained from all patients.

2.2 | Instrumentation

A schematic description of the instrument is presented in Figure 1. A 2-axis scanning galvo-mirror system (GVS012/M, Thorlabs) was coupled to an inverted optical microscope (Nikon Eclipse). A 671-nm wavelength CW laser with maximum power of 250 mW (Gem 671, LaserQuantum) was used for excitation of Raman scattering. A silicon-based CCD detector (Andor Newton 920 BR-DD, Oxford Instruments) attached to a spectrometer (grating blazed for 750 nm, 75% peak efficiency) was used for detection of Raman scattered light. A 2× microscope objective (Nikon Plan Apo 2×/0.1 NA) was used for fast HW Raman spectral imaging to cover a large field of view. The fingerprint Raman spectra were acquired with a high NA 63× oil-immersion objective (RiverD 63× oil/1.2 NA). The scanning area for the galvo-mirror system with the 2× objective was $\sim 7 \times 7$ mm^2 on the sample plane. A translation stage was used to move the sample to achieve larger scanning area covering the entire tissue samples. Scanning tiles were stitched in postprocessing to produce full HW Raman maps of tissue.

Custom-written LabVIEW (National Instruments) software was developed to control the galvo scanners and the microscope translational stage. To achieve high-speed spectral imaging, the program was used in combination with Andor Solis software for data acquisition. A DAQ card (USB-1808X, Measurement Computing) was used to synchronize the movement of the galvo-mirror scanners and for triggering the CCD camera. The acquired data were then processed and analyzed in MATLAB (MathWorks).

3 | RESULTS AND DISCUSSION

3.1 | Instrument optimization and validation

First, different laser wavelengths were evaluated with wavelengths in the visible and NIR regions, to identify the optimal wavelength that may provide efficient excitation of Raman scattering in both fingerprint and high-wavenumber regions, while minimizing the excitation of fluorescence emissions. Although shorter wavelengths (λ) are more advantageous for increasing scattering efficiency (intensity $\sim \lambda^{-4}$) and matching better the spectral response of the silicon CCDs, they can excite fluorescence emission. On the other hand, longer laser wavelengths minimize laser-induced fluorescence emission, but the scattering efficiency is lower, and the CCD will have lower quantum efficiencies. Figure 2 shows Raman spectra of breast tissues, including samples containing both adipose and non-adipose tissue, recorded using three common laser wavelengths: 532, 660, and 785 nm.

The results in Figure 2 show that for 532-nm excitation, the fluorescence background generated by the laser-induced excitation is very high compared to the Raman bands, causing significant distortions or even swamping the Raman bands. For adipose tissue, the CH bands at 2,850–3,010 cm^{-1} in the HW region[6] are detectable, but the signal is on similar scale with the fluorescence background. The fluorescence background is even stronger for nonadipose tissue, and only the broad water band is detectable at $\sim$3,400 cm^{-1}.[19] In the fingerprint region, only the bands at 1,157 and 1,525 cm^{-1} can be detected
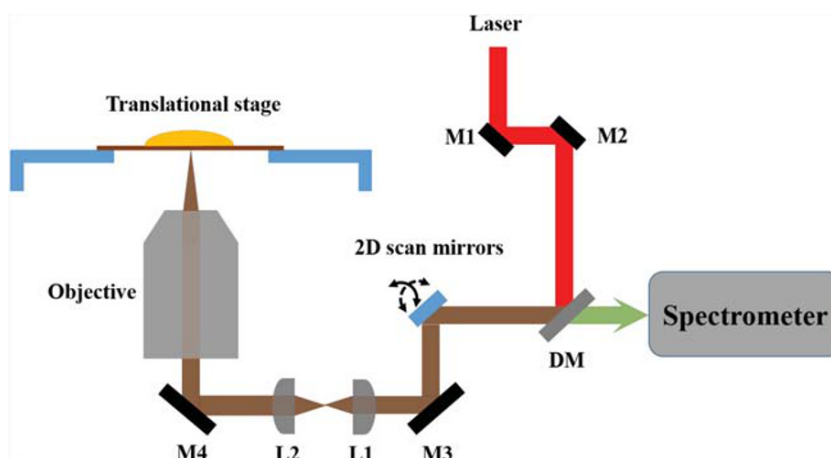
FIGURE 1 Schematic of 2D-galvo-mirror laser scanning system for fast high-wavenumber (HW) Raman imaging and fingerprint Raman spectroscopy using a single 671-nm laser. M1, M2, M3, M4, mirrors; DM, dichroic mirror; L1, L2, lenses
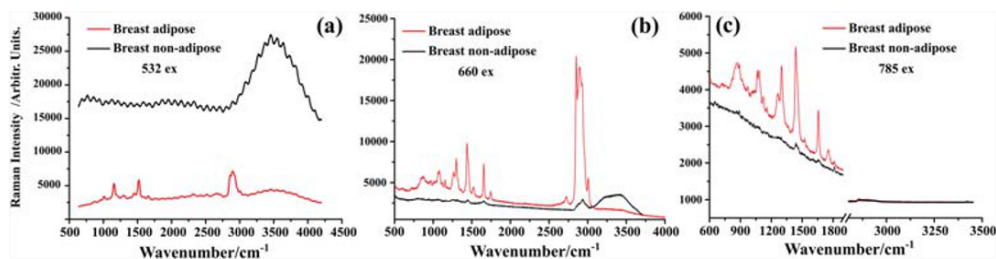
FIGURE 2 Fingerprint and high-wavenumber Raman spectra of breast tissue acquired from adipose tissue and nonadipose tissue (in this case breast tumor). Tumor show strong broad band of O–H in the high-wavenumber region (3,100–3,550 cm^{-1}) due to high water content. Adipose tissue presents much lower level of O–H band, but significant stronger lipid bands (2,800–3,100 cm^{-1})

for the adipose tissue, which can be assigned to carotenoids.[21] For the 660-nm laser excitation, the fluorescence background was significantly reduced and more likely to be caused by light scattering and stray light. The Raman bands are detectable both in the high-wavenumber and fingerprint regions for both adipose and nonadipose breast tissue. In particular, the HW spectra of adipose tissue show intense bands in the 2,700–3,000 cm^{-1} region assigned to CH_2 and CH_3 stretching vibrations. On the other hand, the nonadipose tissue has more intense Raman band in the 3,000–3,550 cm^{-1} region assigned to water stretching vibrations. When the excitation wavelength increases to 785 nm, the background is further reduced, but the Raman bands in the HW region (corresponding to 1,000–1,100 nm) are hardly detectable as the efficiency of the silicon-based CCD detector drops below 30% beyond 1,000 nm. These results indicate that the selection of laser excitation around 660 nm is a good trade-off between maximizing the efficiency for detecting the Raman bands in both fingerprint and the high wavenumber regions and enables discrimination between the adipose and nonadipose tissue. Based on this conclusion, an integrated Raman microscope with a 671-nm laser was developed for all other experiments presented here (671 nm was selected over 660 nm based on availability, laser power, and cost).
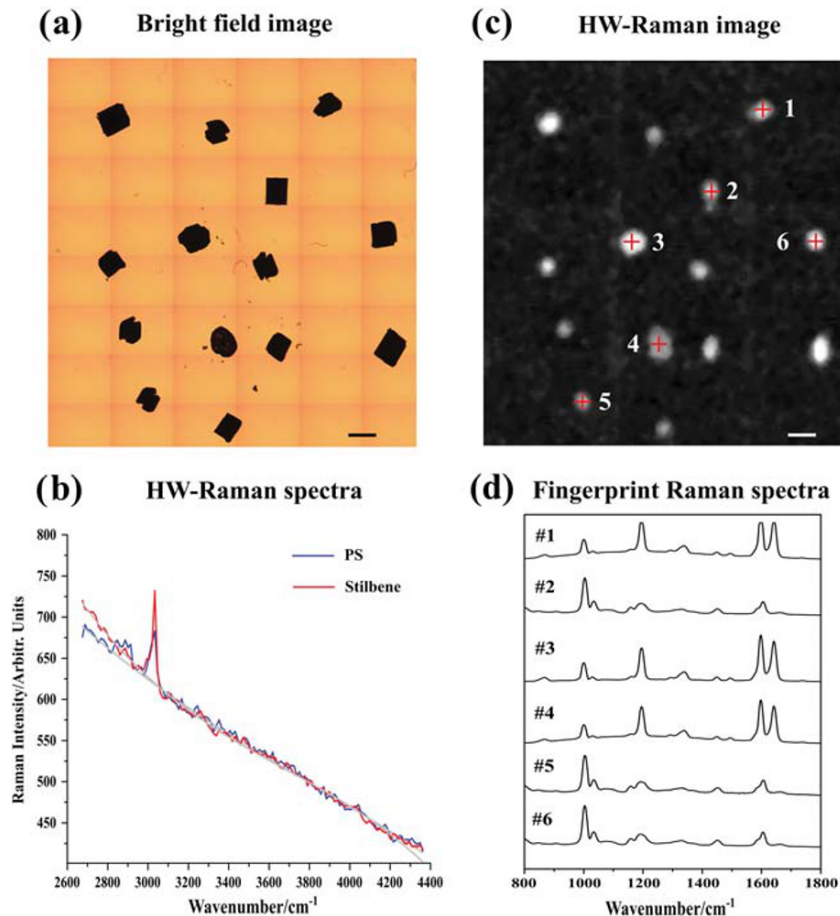
FIGURE 3 (a) Bright field image of PS and stilbene particles. Scale bar: 2 mm. (b) Typical HW-Raman spectra of PS and stilbene obtained during the imaging process; integration time 10 ms/pixel. (c) HW Raman image of the particles shown in (a), constructed using the Raman band at 3,000 cm^{-1}. (d) Fingerprint Raman spectra of PS and stilbene acquired by selecting sampling points based on the HW-Raman map presented in (c)

To maximize the speed for acquiring the HW Raman spectral maps, the field of view was maximized by using a 2× objective (trade-off between field of view and signal strength, which is determined by the numerical aperture of the objective). However, for measuring the Raman spectra in the fingerprint region, the microscope objective was changed to a 63×/NA = 1.2 oil immersion objective optimized for the 650–1,000 nm spectral region. To test the calibration of the instrument when switching between objectives and ensure that the high-wavenumber Raman maps can be used to select regions of the samples that can then be relocated when changing to the higher NA objective, a sample consisting of polystyrene and stilbene particles was used (size of particles ∼2 mm) (Figure 3a). Typical HW Raman spectra of PS and stilbene are shown in Figure 3b, indicating a strong band at ∼3,000 cm^{-1} assigned to C–H stretching vibrations. Figure 3c presents the HW Raman map obtained by integrating the Raman band at 3,000 cm^{-1} after background subtraction (the gray lines in Figure 3b indicate the cubic polynomial fittings for background subtraction). The HW-Raman map was acquired at a resolution of 150 × 150 pixels (step size ∼140 μm), then resized to 9,000 × 9,000 pixels to match the bright field image for calibration. Using the coordinates from the HW Raman map, several particles were selected for measurements of fingerprint Raman spectra (the microscope objective was then changed). Figure 3d shows that the fingerprint Raman spectra acquired at the selected locations agreed with the particle type (polystyrene or stilbene), demonstrating that the relocation accuracy between the HW Raman map and fingerprint Raman measurements is precise within 100 μm, which is sufficient for the purpose of this study.

3.2 | HW Raman mapping of adipose tissue

The optimal parameters for acquiring the HW Raman maps using tissue samples that contained a mixture of adipose and nonadipose tissue were investigated. For convenience, first, we used porcine tissue (abdomen region) from a local supermarket. Figure 4 presents HW Raman maps acquired using a range of acquisition dwell times and spatial steps of ∼230 μm. The selection of the step size was a trade-off between imaging speed and the resolution needed for the clinical application. In this case, the latter is set by considering the smallest types of tumor that need to be detected such as tiny foci of ductal carcinoma in-situ, or a focus of micro invasive carcinoma which are typically less than 1 mm^2 in size. The HW Raman images are constructed by integrating the Raman band at 2,800–3,000 cm^{-1} (assigned to C–H$_2$ and C–H$_3$ symmetric/asymmetric stretching vibrations) after background subtraction and stitching together multiple
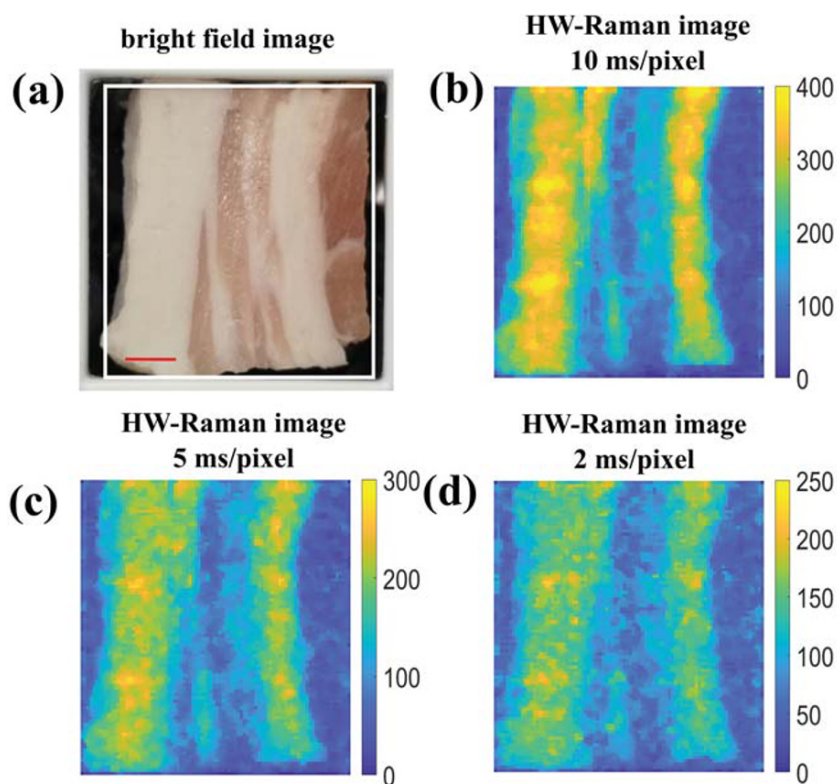
FIGURE 4 HW Raman spectral imaging of pork tissue with different integration times. (a) Bright field image. Scale bar: 4 mm. (b) HW-Raman image with integration time of 10 ms/pixel. Original acquisition size: 90 × 90 pixels, resized to 9,000 × 9,000 pixels. (c) Integration time: 5 ms/pixel. (d) Integration time: 2 ms/pixel

scanning tiles (3 × 3). Figure 4d shows that the adipose tissue can be identified in the HW Raman maps (bright areas) even for dwell times as short as 2 ms/pixel, when laser power of ∼180 mW (at the sample) was used to acquire the spectra. Due to the short dwell time per pixel and low magnification objective, the tissue did not show any evident damage after measurement. Meanwhile, because of the short response time of the galvo-mirrors (400 µs) and high readout rate of the CCD camera (1 MHz/pixel setting and full vertical binning read-out mode), the actual acquisition time was less than 3 min for the entire map, at an integration time of 10 ms per pixel (Figure 4b).

After optimizing the parameters for mapping of adipose tissue from the porcine samples, these parameters were checked using human breast tissue samples. Figure 5 shows HW-Raman images of six breast tissue samples acquired with integration time of 10 ms per pixel, along with the H&E images for comparison.

Similar to the images shown in Figure 4, the HW-Raman images were constructed by integrating the Raman band at 2,800–3,000 cm^{-1} (assigned to C–H$_2$ and C–H$_3$ symmetric/asymmetric stretching) after background subtraction and stitching together multiple scanning tiles (3 × 3). By comparing the HW-Raman images and the corresponding H&E images in Figure 5a–f, the adipose tissues in the breast samples matched well the high-intensity regions in the HW-Raman images. The green circles in Figure 5a–d mark the adipose tissue area in the heterogeneous breast samples (samples contain also other tissue types), whereas in Figure 5e,f correspond to samples containing only adipose tissue. The acquisition time for each of these HW-Raman images (∼21 × 21 mm^2) was only about 3 min, indicating the potential of the HW-Raman imaging system using galvo-mirrors for fast mapping of adipose tissue for human breast samples.
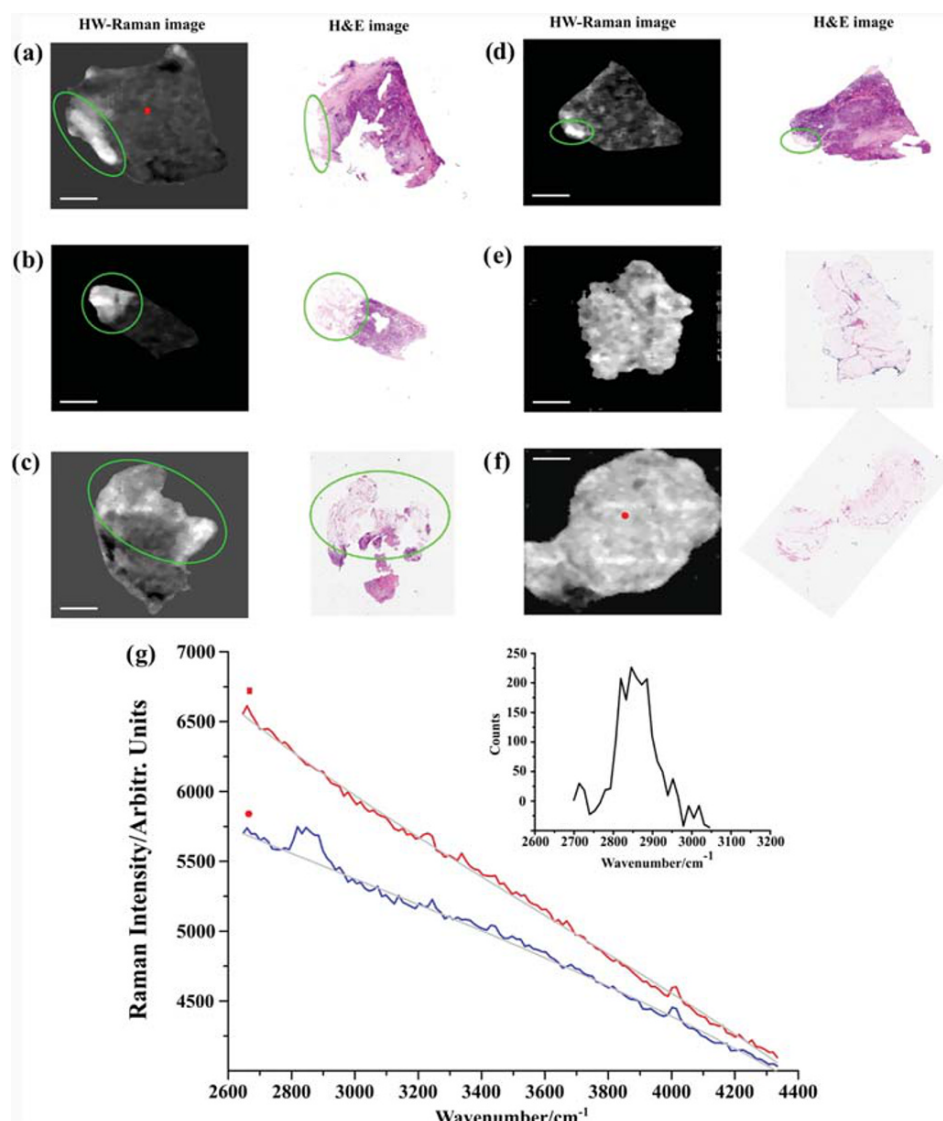
FIGURE 5 (a–f) HW-Raman images of breast tissues (intensity scale: 0–255). H&E images are shown on the right for comparison. Scale bars: 4 mm; (g) HW-Raman spectra of tumor and adipose tissue from the points shown in (a) and (f), sum of 10 pixels; insert graph shows the spectra of adipose tissue after background subtraction

For validation, Figure 5g presents two typical raw Raman spectra in the HW region of nonadipose (red square in Figure 5a) and adipose tissue (red dot in Figure 5f) acquired by the spectral imaging system. The spectra confirm the presence of the CH_2 band in the region of adipose tissue but not in the tumor region. The water band at 3,100–3,550 cm^{-1} cannot be identified, mainly because of the lower intensity and perhaps because the tissue samples were stored in at $-20°C$ (more than a year) prior to the measurement.

3.3 | Integrated HW imaging— Fingerprint Raman spectroscopy for fast analysis of breast tissue

We showed previously[17] that selective-sampling techniques based on intensity threshold segmentation of auto-fluorescence (AF) images and fingerprint Raman spectroscopy measurements are a viable approach for detection of residual tumor in breast resections. This approach minimized the number of fingerprint Raman measurements to achieve faster diagnosis (20–30 min) compared to raster-scanning Raman microscopy (1–2 days). However, one limitation of the AF imaging was that a large number of sampling points for fingerprint Raman spectroscopy were generated in regions of adipose tissue, which is known not to contain tumor. We optimized these algorithms using the HW-Raman images instead of the AF image. HW-Raman has high specificity to adipose tissue, as shown in Figures 4 and 5. As the intensity of the CH_2/CH_3 Raman bands is higher in adipose tissue compared to nonadipose tissue, an intensity threshold can be used to retain only the nonadipose tissue regions and then assign sampling points for fingerprint Raman measurements in these regions only. A typical example is shown Figure 6,

which is a breast sample containing tumor and adipose tissue. The HW-Raman image was generated using the acquired HW Raman spectra and saved as an intensity image with scale of 0–255. By comparing the images with the H&E section, the bright and dark regions in the HW-Raman map correspond to adipose tissue and tumor, respectively. Figure 6c–f shows the generated segments using different intensity threshold values, where the regions of tissue with values higher than the threshold were labelled as adipose tissue, and the areas with values smaller than that threshold as "potential tumor" regions. By comparing the segments in Figure 6c–f to the H&E image, a threshold of 120 was considered sufficient for screening out the adipose tissue and generating sampling points for fingerprint Raman measurements in the "potential tumor" areas. Sampling points for Raman measurements were then generated in the "potential tumor" regions with five points distributed equally in the segments. Previous study[16] has indicated that five samplings per segment are adequate for basal cell carcinoma diagnosis in skin tissue. Certainly, the number of points can be increased if needed for improving accuracy of diagnosis.

We have then investigated the feasibility of combining HW-Raman imaging and fingerprint Raman spectroscopy for fast tumor diagnosis using a single excitation laser. Results in Figure 2 suggested that 671-nm excitation is sufficient to avoid tissue auto-fluorescence in the HW-Raman region while taking good advantage of silicon-based detector in the spectral range of 700–900 nm. The next step was to test if 671-nm excitation is suitable for acquiring Raman spectra in the fingerprint region and discriminating between tumor and other nonadipose tissue structures in breast tissue (e.g., stroma). This was implemented using the segmentation algorithms based on intensity-threshold of HW-Raman maps. Figure 7 presents a typical example for a
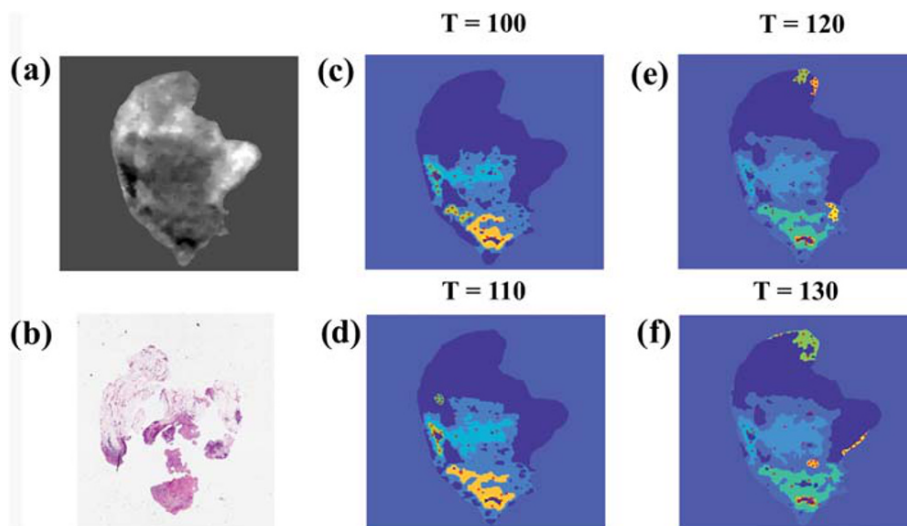
FIGURE 6 HW-Raman imaging and segmentation of breast tumor tissue for selective sampling fingerprint Raman spectroscopy. (a) HW-Raman image (size 2 × 2 cm²); (b) H&E image; (c–f) segmentation of the HW-Raman image with different intensity thresholds from 100 to 130
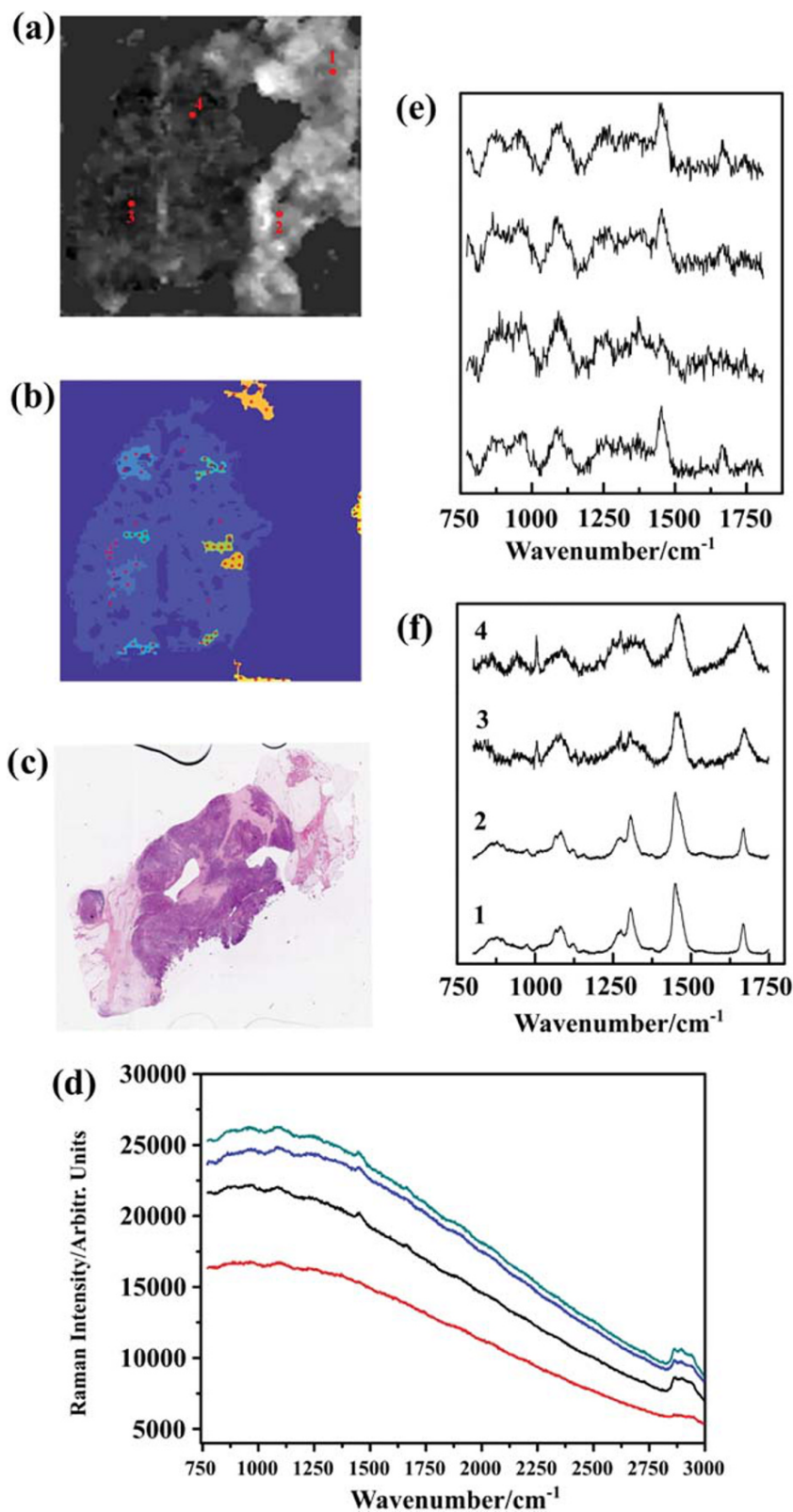
FIGURE 7 Multimodal spectral histopathology diagnosis using high-wavenumber Raman imaging and selective-sampling Raman spectroscopy. (a) HW-Raman image; (b) generated segments and sampling points. (c) Adjacent H&E image; (d) raw Raman spectra obtained using 671-nm excitation at different locations (integration time: 1 s/spectrum); (e) fingerprint Raman spectra obtained using 671-nm excitation, background subtracted; (f) fingerprint Raman spectra obtained using 785-nm excitation (integration time: 1 s/spectrum)

breast tissue sample containing adipose tissue, stroma, and tumor. The comparison between the HW-Raman image and H&E section indicates that the segmentation algorithm was effective in identifying the adipose tissue and allocating sampling points in the areas of stroma and tumor. However, the fingerprint Raman spectra measured at the locations indicated by the sampling points had large backgrounds, likely caused by laser-induced fluorescence or scattering/stray light. Selected Raman spectra, before and after background subtraction, are

reported in Figure 7d,e and show Raman bands at 1,450 and 1,655 cm^{-1} that can be assigned to the CH$_2$ deformations and Amide I vibrations in proteins. However, important bands required for the discrimination of tumor from other nonadipose tissue structures,[14,17] such as nucleic acids (788, 1,098, and 1,342 cm^{-1}) and phenylalanine (1,004 cm^{-1}), are not distinguishable in the spectra. Although the initial test results presented in Figure 2b suggested that lasers with 660 nm wavelength could effectively avoid auto-fluorescence in the fingerprint region, the results on a larger number of samples indicated a high level of sample-to-sample variation. For comparison, fingerprint Raman spectra of the same tissue samples were also measured using 785-nm laser excitation, and typical spectra of adipose tissue and tumor are given in Figure 7f. The spectra were collected from regions of adipose and nonadipose tissue from positions approximately indicated by the red dots in Figure 7a (accurate positions are not available as the sample was moved to another instrument equipped with the 785 nm laser). In this case, the background was significantly reduced, and the Raman bands at 1,004, 1,260, and 1,342 cm^{-1} are well resolved in the spectrum of tumor whereas the Raman spectra from the adipose tissue have the typical bands at 1,297 and 1,450 cm^{-1}, assigned to CH$_2$ and CH vibrations. Although an instrument with a single laser source would be convenient for simplicity, this may not be the most efficient approach. The results suggest that the integration of 671-nm excitation for HW Raman imaging with 785-nm excitation for the fingerprint Raman spectroscopy would be the most appropriate for fast diagnosis of breast cancer.

The ultimate goal is to achieve accurate assessment of whole breast resection specimens within time-scales compatible with intraoperative use in breast conserving surgery. The breast samples used in this study were tissues (4 × 6 mm^2 to 20 × 20 mm^2) cut from whole BCS specimens. In reality, breast resections can have surface area larger than 5 × 5 cm^2. To map the surface of a large specimen with the HW Raman imaging instrument used in this study would require ~15 min. Assuming that ~200 fingerprint Raman spectra would be required to diagnose the regions of nonadipose tissue at the resection surface, the whole analysis time may be completed in ~20–25 min (assuming an integration time of 2–3 s/spectrum to generate a high signal-to-noise ratio spectrum). It is also worth noting that the instrument can be further improved to increase the acquisition speed. The spectrometer and CCD used to acquire HW Raman spectra, although allowed a better understanding of the Raman band intensity relative to the background, had a 5 ms as the shortest time limit required for triggering. Also, when reducing the acquisition times to that level,

the read-out noise of the CCD becomes dominant (2.5 e$^-$/CCD pixel). Replacing the spectrometer/CCD with a single-element detector (e.g., photomultiplier tubes or avalanche photo-diodes) would allow acquisition times below 1 ms (use a filter to detect all Raman photons within the 2,700–2,950 cm^{-1}). These improvements may increase the speed of HW Raman imaging to enable an overall tissue analysis time of ~10 min. If required, additional higher resolution mapping could be carried out at the location of the detected tumor in order to accurately determined the edges.

4 | CONCLUSION

In this study, we evaluated the potential use of integrated high-wavenumber (HW)-Raman imaging and fingerprint Raman spectroscopy for fast intraoperative assessment of surgical margins in breast conserving surgery. A laser scanning Raman imaging system was built using 2D galvo-mirrors to provide spectral imaging in the HW-Raman region. The excitation source (671-nm laser) proved to be suitable to avoid excitation of auto-fluorescence from breast tissue in the HW region while effectively making use of the high quantum efficiency of silicon-based CCDs in the spectral range of 700–900 nm. Results using human breast tissue demonstrated that HW-Raman imaging can accurately identify adipose tissue, which then can be effectively screened from further fingerprint Raman analysis using an intensity-based threshold segmentation algorithm. However, the patient-to-patient variations in the laser-induced background when recording fingerprint Raman spectra, swamping smaller Raman bands required for discrimination of tumor from other nonadipose tissue structures in breast samples. Nevertheless, the auto-fluorescence background was significantly reduced when a 785-nm laser was used, guided by the HW-Raman imaging (acquired with 671-nm laser). These results demonstrate the feasibility of the combined HW Raman imaging and fingerprint Raman spectroscopy for analyzing whole breast specimens resected during surgery, with estimated analysis times of 20–25 min. Further improvements, such as using single element detectors for HW-Raman imaging, may increase further the analysis speed towards intraoperative use.

the Raman microscope for testing different excitation wavelengths.

ORCID

Zhiyu Liao https://orcid.org/0000-0002-6447-5510
Ioan Notingher https://orcid.org/0000-0002-5360-230X

REFERENCES

[1] K. L. Kummerow, L. Du, D. F. Penson, Y. Shyr, M. A. Hooks, *JAMA Surg.* **2015**, *150*, 9.

[2] R. Jeevan, D. Cromwell, M. Trivella, G. Lawrence, O. Kearins, J. Pereira, C. Sheppard, C. Caddy, J. Van Der Meulen, *BMJ* **2012**, *345*, e4505.

[3] J. Landercasper, E. Whitacre, A. C. Degnim, M. Al-Hamadani, *Ann. Surg. Oncol.* **2014**, *21*, 3185.

[4] D. W. Shipp, F. Sinjab, I. Notingher, *Adv. Opt. Photon.* **2017**, *9*, 315.

[5] T. J. E. Hubbard, A. Shore, N. Stone, *Analyst* **2019**, *144*, 6479.

[6] A. S. Haka, K. E. Shafer-Peltier, M. Fitzmaurice, J. Crowe, R. R. Dasari, M. S. Feld, *Proc. Natl. Acad. Sci. U. S. A.* **2005**, *102*, 12371.

[7] I. Barman, N. C. Dingari, A. Saha, S. McGee, L. H. Galindo, W. Liu, D. Plecha, N. Klein, R. R. Dasari, M. Fitzmaurice, *Cancer Res.* **2013**, *73*, 3206.

[8] J. C. Day, N. Stone, *Appl. Spectrosc.* **2013**, *67*, 349.

[9] M. D. Keller, E. Vargis, A. Mahadevan-Jansen, N. de Matos Granja, R. H. Wilson, M.-A. Mycek, M. C. Kelley, *J. Biomed. Opt.* **2011**, *16*, 077006.

[10] N. Stone, R. Baker, K. Rogers, A. W. Parker, P. Matousek, *Analyst* **2007**, *132*, 899.

[11] S. Kang, Y. Wang, N. P. Reder, J. T. C. Liu, *PLoS ONE* **2016**, *11*, e0163473.

[12] C. J. Rowlands, S. Varma, W. Perkins, I. Leach, H. Williams, I. Notingher, *J. Biophotonics* **2012**, *5*, 220.

[13] K. Kong, C. J. Rowlands, S. Varma, W. Perkins, I. H. Leach, A. A. Koloydenko, H. C. Williams, I. Notingher, *Proc. Natl. Acad. Sci. U. S. A.* **2013**, *110*, 15189.

[14] K. Kong, F. Zaabar, E. Rakha, I. Ellis, A. Koloydenko, I. Notingher, *Phys. Med. Biol.* **2014**, *59*, 6141.

[15] F. Sinjab, K. Kong, G. Gibson, S. Varma, H. Williams, M. Padgett, I. Notingher, *Biomed. Opt. Express* **2016**, *7*, 2993.

[16] R. Boitor, K. Kong, D. Shipp, S. Varma, A. Koloydenko, K. Kulkarni, S. Elsheikh, T. B. Schut, P. Caspers, G. Puppels, M. van der Wolf, E. Sokolova, T. E. C. Nijsten, B. Salence, H. Williams, I. Notingher, *Biomed. Opt. Express* **2017**, *8*, 5749.

[17] D. W. Shipp, E. A. Rakha, A. A. Koloydenko, R. D. Macmillan, I. O. Ellis, I. Notingher, *Breast Cancer Res.* **2018**, *20*, 69.

[18] A. Nijssen, K. Maquelin, L. F. Santos, P. J. Caspers, T. C. B. Schut, J. C. den Hollander, M. H. Neumann, G. J. Puppels, *J. Biomed. Opt.* **2007**, *12*, 034004.

[19] E. Barroso, R. Smits, T. Bakker Schut, I. Ten Hove, J. Hardillo, E. Wolvius, R. J. Baatenburg de Jong, S. Koljenovic, G. Puppels, *Anal. Chem.* **2015**, *87*, 2419.

[20] I. S. P. Santos, P. J. Caspers, T. C. Bakker Schut, R. van Doorn, V. Noordhoek Hegt, S. Koljenović, G. J. Puppels, *Anal. Chem.* **2016**, *88*, 7683.

[21] G. J. Puppels, H. S. P. Garritsen, J. A. Kummer, J. Greve, *Cytometry* **1993**, *14*, 251.